Raman Microprobe Analysis of Temperature Profiles in CW Laser Heated Silicon Microstructures

GREGORY D. PAZIONIS, HUA TANG, AND IRVING P. HERMAN, MEMBER, IEEE

Abstract—The use of Raman microprobe analysis to determine temperature profiles in laser-heated microstructures is investigated. As a specific example, steady-state laser heating of silicon disk microstructures on fused silica and sapphire is examined using the 4880 and 5145 Å lines from a argon–ion laser to heat the disk at the center and to probe it with submicrometer spatial resolution. The Stokes shift and line broadening of the Raman microprobe spectra are compared to simulations of the Raman spectra, which utilize temperature profiles calculated by a finite difference analysis of the heat flow equation. The Raman simulation model incorporates the effects of temperature inhomogeneities, strain, and photon-created free carriers within the probed volume; temperature nonuniformity is found to be the most important factor and to be quite significant. In some cases, comparison of experimental and simulated Raman spectra is found to give superior determination of temperature than does the solution of the heat flow equation. This Raman simulation model is also extended to a more general treatment of Raman microprobe analysis of laser-heated microstructures.

I. INTRODUCTION

IN recent years, lasers have become increasingly important in thin-film processing and analysis. Optical diagnostic methods such as absorption and reflection spectroscopies, laser-induced fluorescence, photoluminescence, and Raman scattering have become valuable tools for *in situ* and *ex situ* analysis of thin-film processing. Similarly, laser-assisted chemical processing of metal, semiconductor, and insulator surfaces has attracted considerable interest due to potentially important applications in microelectronics fabrication [1]–[3]. Optical diagnostics have been used for *in situ* probing in a few studies of localized laser surface processing [1]. In one class of laser-assisted surface reactions, namely pyrolytic chemical processes induced by local laser heating of the substrate, the reaction rate depends strongly on the temperature profile. The temperature profile induced by lasers is also important in laser annealing. This paper examines the use of Raman microprobe analysis to determine the temperature profile during laser heating of semiconductor microstructures. Laser heating of silicon microstructures on fused silica and sapphire substrates, of potential importance in microelectronics processing, is used as a specific experimental example. Previous studies of Raman analysis of laser-heated silicon have included work on

bulk substrates [4]–[7], silicon films on sapphire [8], and silicon microstructures produced in direct laser writing [9], [10], as well as the preliminary study of silicon disk microstructures on fused silica [11].

In this investigation, the temperature profiles resulting from laser heating are obtained by matching the experimental Raman spectra with simulated Raman profiles, and they are then compared to the temperature distributions derived by solving the heat flow equation. The temperature profiles derived from the Raman spectra are also checked by determining the laser intensity required to melt the silicon microstructures. In some cases, it is found that Raman spectroscopy may provide a better determination of temperature than the direct solution of the heat flow equation, in large part because of the uncertainties in some of the material properties needed in the calculations.

Laser heating and Raman microprobe experiments are described in Section II. Various configurations are described which utilize either one or two lasers for heating and optical probing. Section III describes a finite difference analysis of heat transfer during steady-state laser heating of silicon microstructures on fused silica and sapphire substrates. This provides the temperature profiles that are used in Section IV to simulate the spectral profiles expected from Raman microprobe analysis of these laser-heated microstructures. The treatment of more general microstructure/substrate systems is also given in Sections III and IV. These simulations show that care must be exercised in interpreting the Raman frequency shifts and linewidths in terms of temperature rises due to laser heating. Comparison of the experiments and Raman simulations for silicon microstructures on fused silica and sapphire substrates is made in Section V, and conclusions on the general usefulness of Raman microprobe determination of temperature are given in Section VI.

II. EXPERIMENT

Circular polycrystalline and epi silicon microstructures (undoped), 0.62 μm thick, were fabricated on substrates that are transparent in the visible, and were used in the laser heating studies. In one set of samples, microstructures were made from polycrystalline Si films deposited by chemical vapor deposition (CVD) on fused silica and (randomly aligned) sapphire flats in one facility, and are designated poly-1. A second set of samples was made using polycrystalline Si films that were deposited on

(1102) aligned sapphire flats in a different CVD facility (poly-2). Microstructures were also fabricated from epi-Si films on (1102) aligned sapphire substrates (epi) that were supplied by a vendor. These films were patterned by photolithography using the same photomask for all samples. Because of the isotropic process used to etch the silicon films, the disk-shaped microstructures made from 6, 15, and 25 μm diameter features produced ~4.0, 13.4, and 23.4 μm diameter disks with sloping edges, which were employed in the heating experiments.

The laser lines of an argon laser operating in multiline mode are first dispersed by a prism, then the undesired lines are blocked, and finally the remaining lines are recombined by a second prism. Either the 4880 or the 5145 Å line is selected for laser microheating and microprobing, or sometimes both of these lines are selected by this apparatus for simultaneous use in the experiments. The laser beam is then focused on the microstructure, usually at the center, with an infinity-focus-corrected 20× microscope objective mounted on a z translation stage, and the substrates are mounted in air on a large heat sink atop an x-y translation stage. The spot size and ellipticity of the laser at the focus are measured by monitoring the laser power transmitted through the silicon disk with a photodiode placed within the stage beneath the transparent substrate, while laterally translating the edge of the disk (x or y direction) across the focus. This procedure also enabled precise relative alignment in the two-beam experiments reported below and in an earlier report [11]. The beam radius w (half width at the $1/e$ intensity points) at the focus is typically 0.56 μm; the difference in beam radius in orthogonal directions is less than 0.05 μm.

In one-beam experiments, the laser both heats the disk and acts as a source of photons for Raman scattering. In two-beam experiments, one beam has variable intensity and is focused in the center of the microstructure (5145 Å), while the second beam is very weak, has a different wavelength (4880 Å), and is scanned across the microstructure by adjusting a beam steering mirror. The second beam (the probe) serves as a Raman probe of temperature across the disk, but does not heat the disk significantly, while the first beam (the heating laser) both heats the disk and monitors the temperature at the disk center. For either the one- or two-beam arrangement, Stokes or anti-Stokes radiation is detected after dispersion by a spectrometer using an intensity-enhanced diode array. When 4880 and 5145 Å lines are both used, the Stokes-shifted radiation of 4880 Å (near 5007 Å) and the anti-Stokes radiation of 5145 Å (near 5011 Å) can be monitored simultaneously by the diode array, as reported in [11].

The Raman spectra of these samples were initially examined and compared to c-Si at laser powers low enough (< 1 mW) that laser heating can be ignored. The optical phonon frequency of the poly-1 structures of fused silica were downshifted by about 1.5 cm^{-1} relative to c-Si (520.5 cm^{-1}), while on the sapphire substrates, the frequency was relatively upshifted by about 1 cm^{-1} for poly-1 and by about 2 cm^{-1} for both poly-2 and epi silicon
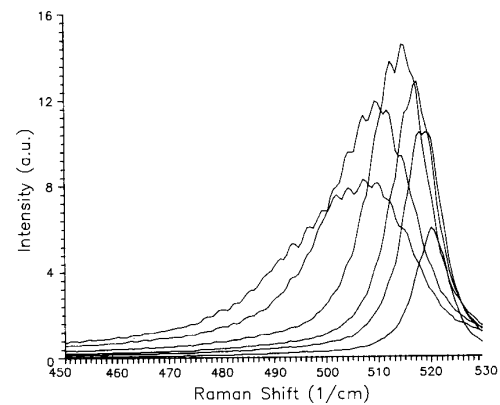

Fig. 1. Stokes Raman spectra of 4 μm diameter poly-2 silicon disks atop sapphire in one-beam heating and probing experiments with 5145 Å. The curves, from right to left, were obtained with laser powers 20, 30, 40, 60, 75, and 90 mW, respectively, and a 0.56 μm spot size.

samples. Usually, the magnitude of these shifts was slightly smaller for the smaller diameter disks than for the larger disks. The linewidths (FWHM) of the low-power spectra were about 6 cm^{-1} broader for poly-1 on fused silica than the c-Si linewidth (2.9 cm^{-1}), while for structures on sapphire, the linewidths were broader by about 6.5 cm^{-1} for poly-1 and about 2 cm^{-1} for both poly-2 and epi silicon than for c-Si. The instrumental contribution to the linewidth, ~2.5 cm^{-1}, is removed from all reported data.

Fig. 1 displays the Stokes spectra in one representative example of one-beam laser heating, using the 5145 Å laser line with a power ranging from 20 to 90 mW focused on a 4 μm diameter poly-2 silicon disk atop sapphire. For increasing laser power, the Stokes shift decreases and the profile linewidth increases. As discussed in some detail below, this indicates that the microstructure temperature is increasing monotonically with laser power. Blackbody radiation did not contribute significantly to the background in any of the reported Raman measurements.

Fig. 2 displays the (a) Stokes shift and (b) linewidth at the center of 4 and 13 μm polysilicon microstructures on fused silica, as a function of the heating laser power (4880 Å) in one-beam heating and probing experiments; the Raman profiles for 23 μm structures are very similar to those for the 13 μm disks. The laser power was increased until melting of the Si disk was observed (~22 mW for the 4 μm disks and about 28 mW for the larger disks). These melting conditions are used to check the temperature profiles in Section V. In all cases examined, here and below, the Raman shifts and linewidths obtained from Stokes spectra and the corresponding anti-Stokes spectra were the same. (This need not be true when structures are inhomogeneously heated and when the Raman scattering intensity depends strongly on temperature). These shifts and linewidths are used in Sections IV and V to obtain the peak temperatures and the temperature profiles in the laser-heated structures. The Stokes/anti-Stokes intensity ratios are also readily obtained here. However, use of these ratios to determine temperature appears to be relatively un-
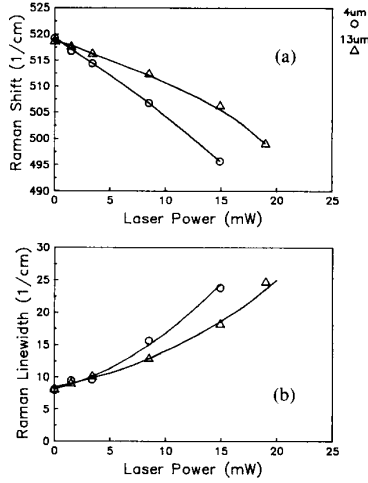
Fig. 2. Stokes Raman (a) shifts and (b) linewidths (FWHM) of poly-1 silicon disks on fused silica as a function of laser power (4880 Å) in one-beam experiments. The disk diameters are 4 μm (circles) and 13 μm (triangles).
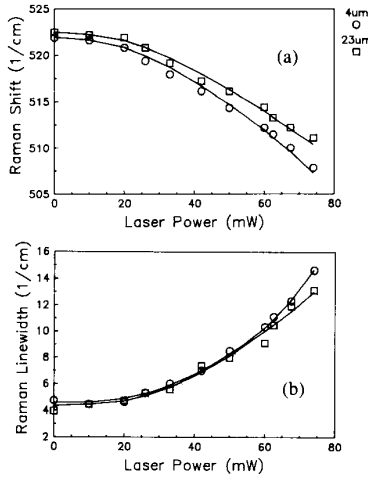

Fig. 3. Stokes Raman (a) shifts and (b) linewidths (FWHM) of poly-2 silicon disks on sapphire as a function of laser power (5145 Å) in one-beam experiments. The disk diameters are 4 μm (circles) and 23 μm (squares).

reliable for both one-beam and two-beam experiments, and it is not employed here [11].

Analogous plots for one-beam heating and probing of 4 and 23 μm diameter poly-2 Si microstructures on sapphire are shown in Fig. 3; data for 13 μm disks are the same as for 23 μm disks. The laser power required to melt the silicon structures was about 110 mW for each of these three disks. The Stokes spectra were also examined for 4 μm poly-1 and epi silicon disks on sapphire, giving spectral data that were qualitatively similar to that in Fig. 3. However, the Raman shift decreased and the linewidth increased with laser power faster for poly-1 disks and slower for epi disks vis-à-vis poly-2 disks. Also, the laser power needed to melt the structures was lower for poly-1 (~ 80 mW) and higher for epi samples (~ 300 mW), relative to the power needed to melt poly-2 disks.
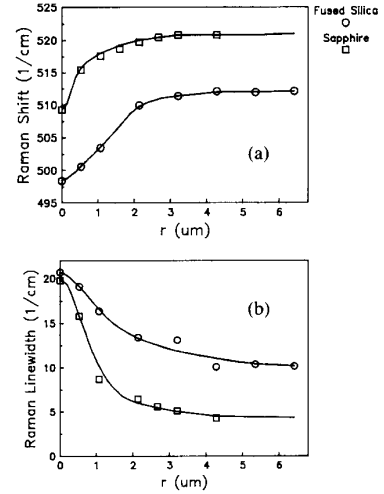

Fig. 4. Stokes Raman (a) shifts and (b) linewidths (FWHM) from two-beam experiments on a 13 μm diameter poly-1 disk on fused silica (circles) and a 13 μm diameter poly-2 disk on sapphire (squares) as a function of the radial displacement (μm) of the probe laser from the center. The power of the fixed heating laser (5145 Å) is 15.4 mW for the fused silica case and 90 mW for sapphire, while the power of the probe laser (4880 Å) is ≤1 mW. Data from the 5145 Å anti-Stokes spectra are used at $r = 0$, while the 4880 Å anti-Stokes spectra are used for $r > 0$.

Two-beam experiments were conducted for 13 μm diameter polysilicon disks on fused silica (poly-1) and sapphire (poly-2). The power of the pump laser (5145 Å), which is fixed at the center, was 15.4 mW for the fused silica substrate and 90 mW for sapphire, while the power of the probe laser (4880 Å) was ≤1 mW. The Raman shifts and linewidths from these spectra are plotted in Fig. 4(a) and (b), respectively, versus the radial displacement of the probe from the center.

III. TEMPERATURE CALCULATION

The temperature profile is calculated by solving the heat flow equation in steady state:

$$\vec{\nabla} \cdot \left(K(T)\vec{\nabla}T \right) + H = 0 \tag{1}$$

where T is the temperature, K is the thermal conductivity, and H is the local heat source due to laser absorption in the deposited disk:

$$H(r, z) = \alpha\left(T(r, z)\right)\left[1 - R\left(T(r, 0)\right)\right]I_l^o(r, 0)$$

$$\cdot \exp\left[-\int_0^z \alpha\left(T(r, z)\right) dz\right]. \tag{2}$$

In (2), α is the deposit absorption coefficient, R is the reflectivity at the deposit/air interface, and $I_l^o(r, 0)$ is the intensity profile of the incident focused heating laser. The disk thickness is assumed to be much smaller than the Rayleigh range. With an incident laser power P and the laser in a Gaussian TEM$_{00}$ mode with spot size w_h (half width at $1/e$ intensity points), the intensity profile of the incident laser is

$$I_l^o(r, 0) = \frac{P}{\pi w_h^2} \exp\left(-r^2/w_h^2\right). \tag{3}$$

Equation (1) is solved numerically by finite difference methods for silicon disks of diameter d and thickness h on transparent substrates which are immersed in air. The heating laser is assumed to be at the center, so there is radial symmetry. r is the radial coordinate from the center of the disk, while z is the distance down from the top of the disk, so the disk/substrate interface is at $z = h$. The boundary conditions at each interface, including the interfaces with air, are provided by the continuity of heat flow, and T is set to 300 K for $r = \infty$ and $|z| = \infty$. More details of the finite difference calculation may be found in [12].

Part of the Gaussian beam laser is transmitted through the surface at $z = 0$. The attenuation of the laser is tracked during the propagation through the disk (versus z) for each r as given in (2). The beam is assumed to be totally transmitted at the deposit/substrate interface at $z = h$. Neglecting reflection of the attenuated beam at this interface leads to an underestimate of the temperature rise in silicon by less than 10 percent at low temperatures, and by less than 1 percent for peak disk temperatures >900 K, for which $\alpha h \gg 1$.

The derived temperature distributions are very sensitive to the thermal and optical material parameters used in the calculation. These parameters may vary with temperature and laser wavelength, and may depend on the crystallinity of the materials. Small uncertainties in these parameters, as well as in the measurements of the incident laser power, the beam radius at the focus, and the diameter of the disk microstructures will lead to inaccurate temperature profiles. Disk diameters were measured by scanning electron microscopy and by monitoring the transmission of a weak focused laser through the structures as a function of lateral position. Temperature profiles are calculated using the parameters specific to the experiments reported in Section II and also for a more general parameterization. The beam radius obtained in the experiments, $w = 0.56 \mu m$, is used in all temperature calculations and Raman spectrum simulations, as is the film thickness $h = 0.62 \mu m$.

The thermal conductivities used for air [13] and for the substrates (K_s) fused silica [14] and sapphire [15] are

$$K_{air} = 1.049 \times 10^{-4} + 5.647 \times 10^{-7} T \text{ W/cm} \cdot \text{K} \tag{4}$$

$$K_{fused\,silica} = \begin{cases} 0.006735 \, T^{0.1479} & 300 < T < 700 \text{ K} \\ 0.006970 \, T^{0.1468} & 700 < T < 1200 \text{ K} \\ 0.001647 \, T^{0.3630} & 1200 < T < 1690 \text{ K} \end{cases}$$
$$\text{W/cm} \cdot \text{K} \tag{5}$$

$$K_{sapphire} = a + \frac{b}{T - c} \text{ W/cm} \cdot \text{K}$$

$$\text{with } a, b, c = \begin{array}{ll} -0.0385886, \, 118.7572, \, -42.317381 & 300 < T < 700 \text{ K} \\ 0.04538, \, 25.2930, \, 357.0437 & 700 < T < 1200 \text{ K} \\ 0.0753851, \, 0, \, 0 & 1200 < T < 1690 \text{ K.} \end{array}$$

The thermal conductivity of the deposit disk is K_d. For c-Si, the thermal conductivity is [16]

$$K_d = K_{c\text{-}Si}(T) = \frac{299}{T - 99} \text{ W/cm} \cdot \text{K.} \tag{7}$$

There have been relatively few studies of the thermal conductivity of polycrystalline Si [17]. At room temperature, it is between 0.5–$0.8 \times$ that of crystalline silicon, while at higher temperatures, it apparently approaches $K_{c\text{-}Si}(T)$. The exact dependence depends on grain size and method of preparation.

The surface reflectivity $R(T)$ of c-Si is used here for both crystalline and polycrystalline Si [18]:

$$R(T) = 0.367 + 4.29 \times 10^{-5} T. \tag{8}$$

Jellison and Modine [19] have measured the absorption coefficient for c-Si at the two argon–ion laser wavelengths used here as a function of temperature:

$$\alpha(T) = \alpha_{c\text{-}Si}(T) =$$
$$0.628 \exp(T/433) \quad 1/\mu m \text{ for 5145 Å}$$
$$0.907 \exp(T/438) \quad 1/\mu m \text{ for 4880 Å.}$$
$$\tag{9}$$

At room temperature, the absorption coefficient of polycrystalline silicon is about $3\times$ that of c-Si in the visible [20], [21]. This was confirmed in this study by transmission of the laser through the silicon disks. It is assumed here that for all T,

$$\alpha_{poly\text{-}Si}(T) = 3\alpha_{c\text{-}Si}(T). \tag{10}$$

A series of temperature calculations were performed for laser heating of $4.0 \mu m$ diameter disks on transparent substrates, in which the disks are assumed to have the optical properties of c-Si and the thermal conductivity of the deposit K_d and the substrate K_s are assumed to be independent of temperature. Within each set of runs in this parameterization, the ratio K_d/K_s is set equal to a constant and the laser power is varied. For purposes of comparison, K_d is always set equal to $K_{c\text{-}Si}(T = 300 \text{ K}) = 1.5$ W/cm $\cdot$ K. In Fig. 5(a), the radial temperature profile on the top of the disk ($z = 0$) is plotted for K_d/K_s ranging from 0.2 to 50. The laser power P in each case has been chosen so that the peak temperature rise T_{max} (T at $r = 0$, $z = 0$) is about 1550 K. Under these conditions, T_{max} versus P is fairly linear for each K_d/K_s ratio. Fig. 5(b) displays the results of these calculations at the bottom of the disk, at $z = h = 0.62 \mu m$.
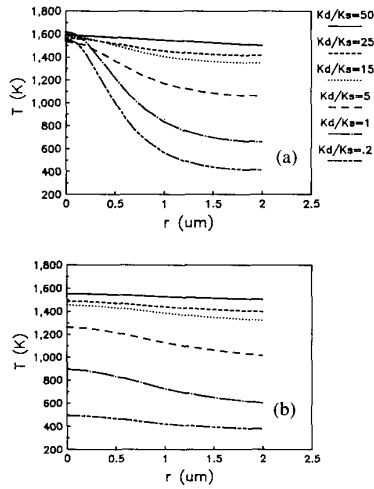
Fig. 5. The calculated temperature profiles versus radial displacement (μm) for the test case of 4 μm disks, having the optical properties of c-Si, on transparent substrates (a) at the top of the disk ($z = 0$) and (b) at the bottom of the disk ($z = h = 0.62$ μm, the deposit/substrate interface). The parameters for the runs are $K_d/K_s = 50, 25, 15, 5, 1$, and 0.2 (respectively corresponding to the curves with decreasing temperature at $r = 2$ μm) with laser powers 50, 90, 140, 300, 700, and 1000 mW, respectively. The thermal conductivity is assumed to be independent of temperature, and the laser powers were chosen so $T_{max} = T(r = 0, z = 0)$ is about 1550 K.
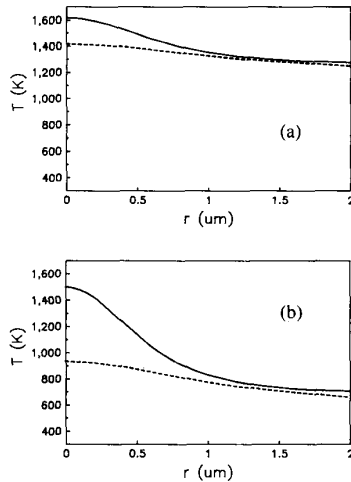

Fig. 6. The calculated temperature profiles versus radial displacement (μm) for 4 μm diameter polysilicon disks for the top of the disk ($z = 0$, solid line) and bottom of the disk ($z = 0.62$ μm, dashed line) for a (a) fused silica substrate (24 mW, 4880 Å) and a (b) sapphire substrate (5145 Å, 100 mW).

Fig. 5 exhibits several trends. When the substrate thermal conductivity is much smaller than that of the disk (K_d/K_s large), the temperature profile is relatively uniform in the r and z directions, and large temperature increases are attainable with relatively low laser power. In contrast, when the thermal conductivity of the substrate is comparable to that of the disk, the temperature profile is very nonuniform in both the r and z directions, and relatively high powers are required to achieve the same

T_{max} possible with small K_s. These results are in agreement with similar calculations reported by Piglmayer *et al.* [22]. Note that the thermal profile for $K_d/K_s = 1$ approximates that for a uniform substrate.

The temperature profiles in Fig. 5 slightly exaggerate the importance of the temperature inhomogeneities during Raman microprobe analysis in one-beam heating since the beam radius (0.56 μm) is much smaller than the disk radius (2.0 μm) and the penetration depth for laser and Stokes radiation is much smaller than the disk thickness $h = 0.62$ μm at elevated T [(9) and (10)].

Similar temperature calculations were performed for silicon disks on fused silica and sapphire, using the temperature-dependent thermal conductivities for these substrates and for silicon (5)–(7). Fig. 6(a) displays one such result for the radial temperature profile at the top and bottom of a 4.0 μm diameter polysilicon disk on fused silica ($P = 24$ mW, 4880 Å), and Fig. 6(b) shows the calculation for the same disk on sapphire ($P = 100$ mW, 5145 Å). As expected from their relative thermal conductivities, laser-heated silicon disks on fused silica have a fairly uniform temperature profile, especially within the probing volume in one-beam experiments, while for silicon on sapphire, the profile is quite inhomogeneous.

IV. RAMAN SPECTRUM SIMULATION

The spectral differential cross section for Stokes scattering from the laser frequency ω_l to the Stokes frequency $\omega_s = \omega_l - \omega_p$ is [23], [24]

$$\frac{d^2\sigma}{d\Omega \, d\omega_s} = A \frac{\omega_l \omega_s^3 v}{\omega_p} \left(\frac{\eta_s}{\eta_l}\right) |\chi(\omega_l, -\omega_p, T)|^2$$

$$\cdot [n(\omega_p) + 1] g(\omega_s) \tag{11}$$

where A is a constant, v is the local scattering volume, η is the index of refraction, χ is the polarization-averaged Raman susceptibility, n is the phonon occupation number $1/[\exp(\hbar\omega_p/k_B T) - 1]$, ω_p is the local optical phonon frequency, and $g(\omega_s)$ is the lineshape. The subscripts l and s refer to the probing laser and Stokes radiation, respectively. The Raman lineshape is given by

$$g(\omega_s) = \frac{\Gamma_p(T)/2\pi}{\left[\omega_s - \left(\omega_l - \omega_p(T)\right)\right]^2 + \left[\Gamma_p(T)/2\right]^2} \tag{12}$$

where Γ_p is the local linewidth (FWHM).

The Raman spectrum of c-Si uniformly heated in an oven has been studied by several groups, including Balkanski *et al.* [25] who have modeled the experimental temperature dependence of the Raman shift ω_p and linewidth Γ_p (FWHM) for the TO mode in c-Si as

$$\omega_p^{c\text{-}Si}(T) = \omega_o - 2.96\left(1 + \frac{2}{e^x - 1}\right)$$

$$- 0.174\left(1 + \frac{3}{e^y - 1} + \frac{3}{(e^y - 1)^2}\right) \text{cm}^{-1} \tag{13}$$

$$\Gamma_p^{c\text{-Si}}(T) = 1.295\left(1 + \frac{2}{e^x - 1}\right)$$

$$+ 0.105\left(1 + \frac{3}{e^y - 1} + \frac{3}{(e^y - 1)^2}\right) \text{cm}^{-1}$$

$$\tag{14}$$

where

$$x = \frac{\hbar\omega_o}{2k_B T}, \quad y = \frac{\hbar\omega_o}{3k_B T}, \quad \text{and} \quad \omega_o = 528 \text{ cm}^{-1}.$$

The local phonon frequency and linewidth ω_p and Γ_p may differ from $\omega_p^{c\text{-Si}}$ and $\Gamma_p^{c\text{-Si}}$ because of local perturbations, such as those caused by strain.

The expression for the silicon Raman Stokes suscepti-bility for subdirect bandgap radiation given in [23] is used in (11):

$$\left|\chi(\omega_l, -\omega_p, T)\right|^2 = A' \exp\left(T/390\right) \tag{15}$$

where A' is a constant.

Experimentally, the photon scattering rate is directly measured:

$$\frac{d^2\bar{R}}{d\Omega\, d\omega_s} = \frac{I_l}{\hbar\omega_l} \frac{d^2\sigma}{d\Omega\, d\omega_s} \tag{16}$$

where I_l is the intensity of the probe laser.

Raman analysis of laser-heated silicon films must in-clude several factors absent in oven-heated c-Si. Laser heating leads to a nonuniform temperature profile (Figs. 5 and 6), and therefore the local phonon frequency and linewidth are functions of position. The relative position of the probe and heating lasers is significant, as is the penetration depth of the probe into the film. The Raman spectrum may also be perturbed from built-in strain of the silicon film on the substrate [26], [27] and from thermally induced strains [28]. For very small grain sizes (<200 Å), the Raman shift of polysilicon is somewhat smaller and the lineshape more asymmetric than for crystalline silicon [29]. Because the low-laser power Raman line-shapes of the poly-2 and episilicon disks on sapphire are very similar and because large-grained polysilicon is ex-pected to form at the CVD deposition temperatures used here, the low-power Raman spectrum of stress-free poly-silicon and c-Si are assumed to be the same. Furthermore, since high densities of electrons or holes perturb the Ra-man profile in silicon [30], [31], the high steady-state concentration of electron-hole pairs created during visi-ble laser heating of even intrinsic silicon may also perturb the Raman profile. As is seen below, temperature inho-mogeneity appears to be the major influence on the Ra-man spectrum.

In Raman microprobe analysis of a silicon disk with radius $d/2$ and thickness h, the measured scattering rate is obtained by integrating the flux of scattered photons throughout the disk:

$$\frac{d^2\bar{R}}{d\Omega\, d\omega_s} = \int_0^h \int_0^{d/2} \frac{A''\omega_s^3}{\eta_l\eta_s\omega_p}\left[t(r, z)\, I_l(r, z)\right]$$

$$\cdot \left|\chi(\omega_l, -\omega_p, T)\right|^2 [n(\omega_p) + 1]$$

$$\cdot g(\omega_s) 2\pi r\, dr\, dz \tag{17}$$

where A'' is a constant and $I_l(r, z)$ is the local intensity of the probe laser:

$$I_l(r, z) = \left(1 - R_l(r, 0)\right) I_l^o(r, 0)$$

$$\cdot \exp\left[-\int_0^z \alpha_l(T(r, z))\, dz\right] \tag{18}$$

with R_l the probe reflectivity, I_l^o the incident laser inten-sity, α_l the probe laser absorption coefficient, and $t(r, z)$ the trapping factor for the Stokes radiation:

$$t(r, z) = \left(1 - R_s(r, 0)\right) \exp\left[-\int_0^z \alpha_s(T(r, z))\, dz\right].$$

$$\tag{19}$$

Note that (2) tracks the absorption of the heating laser through the disk, while (18) does the same for the probe laser. The probe laser is also assumed to be a TEM$_{00}$ Gaussian beam, which is centered at $r = 0$ for one-beam heating and probing, and is radially displaced from the center when a second, scannable laser is used as the probe; in this latter case, (17) is extended to an integral over r, θ, and z.

Temperature inhomogeneities are included in expres-sion (17) by using the local Raman shifts $\omega_p(T(r, z))$ and linewidths $\Gamma_p(T(r, z))$ in the integration over the probed volume. Possible effects due to strain, degree of crystal-linity, and free carriers are included by their effect on the local values of ω_p and Γ_p, which are perturbed from the values given in (13) and (14). In the Raman simulations, (8)–(10) are used for the reflectivity and absorption coef-ficients at 4880 and 5145 Å. Reference [19] is used to obtain the optical constants at the Stokes wavelengths.

The experimental and simulated Raman spectra can be characterized by the frequency shift of the peak ω_{pk} and the full width at half maximum of the spectrum Γ_{pk}. Al-ternately, these parameters can be converted into effective temperatures T_ω and T_Γ by solving for these temperatures in $\omega_{pk} = \omega_p(T_\omega)$ and $\Gamma_{pk} = \Gamma_p(T_\Gamma)$ using (13) and (14), respectively, or slightly modified versions of these equa-tions which include effects such as built-in strain pertur-bations. The relation between T_ω and T_Γ and the temper-ature distribution will be made below.

A. Temperature Inhomogeneity

There are large temperature inhomogeneities along both the r and z directions in the general case of laser heating of silicon disks discussed in Section III; this is also true for silicon films on substrates. When the thermal conduc-

tivity of the deposit is much greater than that of the substrate, as for silicon on fused silica, the temperature distribution within the disk deposit is fairly uniform and averaging effects within the probed volume are relatively unimportant [11]. When K_d/K_s is on the order of one or smaller, temperature profile variations in the probed volume are large. In this case, if the spot size of the probe laser w_l is much smaller than the heating laser spot size w_h, then much of the averaging in the radial direction is eliminated. If the spot size of the probe laser is much greater than the probe wavelength λ_l, then this radial direction averaging can also be removed by spatial imaging of the collected Raman radiation [8]. Averaging in the z direction can be lessened by choosing λ_l so that the absorption depth $1/\alpha_l$ is minimized. Unless otherwise specified, the spot sizes of the heating and probing lasers are assumed to be $w_h = w_l = 0.56$ μm, as in the experiments reported in Section II.

A parametric investigation of Raman simulations for one-beam laser heating and probing was performed for a range of laser powers. Raman simulations of the parameterized test cases described in Fig. 5 and the experimental examples of polysilicon disks on fused silica and sapphire are obtained by inserting the temperature profiles (calculated in Section III) into (17). Fig. 7(a) and (b) depict representative examples of these simulations, showing the spectra for silicon on fused silica and sapphire substrates, respectively. Note the similarity of the experimental and simulated spectra obtained in one-beam laser heating of silicon disks on sapphire in Figs. 1 and 7(b), respectively. This similarity is also true for laser heating of silicon microstructures on fused silica.

Within the parameterized Raman simulation runs, the thermal conductivity ratios were $K_d/K_s = 1$, 5, and 50, and the absorption coefficients and Raman scattering probabilities of crystalline silicon were assumed. The effective temperatures T_ω and T_Γ were obtained from these simulations using (13) and (14), respectively, and are plotted in Fig. 8 versus the maximum temperature of the disk $T_{max} = T(r = 0, z = 0)$. The laser power is an implicit variable in this figure.

When the thermal conductivity of the deposit is much greater than that of the substrate ($K_d/K_s = 50$), T_ω, T_Γ, and T_{max} are all very nearly equal because the temperature distribution in the probed volume, and in fact throughout the whole disk, is very uniform. This changes dramatically when the thermal conductivity of the deposit becomes comparable to that of the substrate. For $K_d/K_s = 1$ and $T_{max} = 1300$ K, the average shift of the Raman profile ω_{pk} gives a much lower effective temperature $T_\omega = 1000$ K, while the linewidth Γ_{pk} gives a much higher temperature $T_\Gamma = 1600$ K than T_{max}. Interpreting either one of these effective temperatures as the maximum disk temperature leads to a 300 K error. However, determination of T_ω or T_Γ from an experimental or simulated Raman profile, coupled with the use of Fig. 8 as a calibration curve, yields the correct maximum value of the temperature profile T_{max}. In general, the appropriate calibration plot can
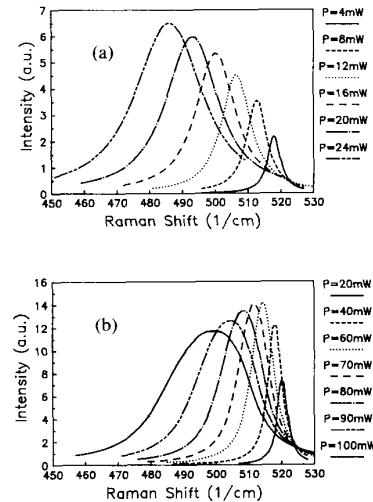

Fig. 7. Simulated one-beam Raman profiles for 4 μm polysilicon disks on (a) fused silica (4880 Å) and (b) sapphire (5145 Å), with a 0.56 μm laser spot size and the listed laser powers increasing for the curves going from right to left.
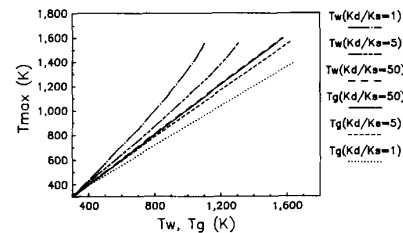

Fig. 8. Maximum disk temperature T_{max} as a function of the effective temperature, derived from the simulated Raman profile peak frequency shift [T_ω (Tw in figure)] or linewidth [T_Γ (Tg in figure)], for the test cases of 4 μm diameter disks with $K_d/K_s = 1$, 5, and 50, using Fig. 5.

be derived by computation when the microstructure/substrate geometry and thermal conductivities are known, as in the case here, or in some examples, a calibration plot can even be deduced by comparing the experimental values of T_ω and T_Γ that are obtained for a range of laser powers. When the thermal conductivities depend on temperature, the calibration curves can differ qualitatively from those in Fig. 8, as is seen below.

Equivalently, T_{max} can be obtained directly from a Raman spectrum using calibration plots of the peak frequency and linewidth of the simulated spectra (ω_{pk} and Γ_{pk}) versus T_{max}, without the intermediate step of conversion to T_ω and T_Γ. The data in Fig. 8 are replotted in this manner in Fig. 9.

Qualitatively, these averaging effects can be understood by considering a temperature profile with a given T_{max} and a temperature variation of about $\Delta T(>0)$ within the probed area. Assuming that the phonon frequency ω_p and linewidth Γ_p vary linearly in temperature, the peak frequency of the averaged Raman profile is

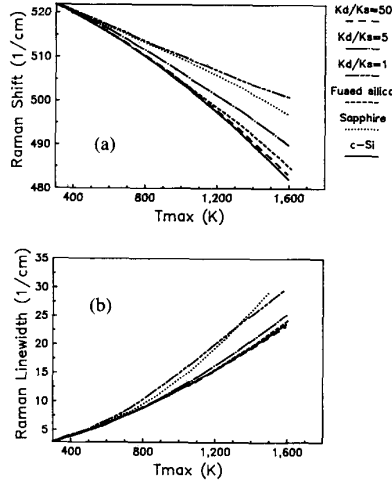$$\omega_{pk} = \omega_p(T_{max}) - a\frac{d\omega_p}{dT}\Delta T \qquad (20)$$

Fig. 9. The (a) peak frequency shift ω_{pk} and (b) linewidth Γ_{pk} (FWHM) of the simulated Raman spectra versus T_{max} for the 4 μm diameter disk test cases $K_d/K_s = 0.2, 1, 5, 50$, and 4 μm silicon disks on fused silica and sapphire, and also uniformly heated c-Si [using (13) and (14)]. Using this figure, T_{max} may be derived from either ω_{pk} or Γ_{pk}.

and the linewidth is

$$\Gamma_{pk} = \Gamma_p(T_{max}) - b\frac{d\omega_p}{dT}\Delta T \qquad (21)$$

where a and b are on the order of unity. If this measured profile were assumed to be from uniformly heated silicon, then the temperature T_ω deduced from the Raman shift ω_{pk} would be

$$T_\omega = T_{max} - a\Delta T \qquad (22)$$

while from the linewidth Γ_{pk}, the temperature T_Γ would be

$$T_\Gamma = T_{max} - \frac{\dfrac{d\omega_p}{dT}}{\dfrac{d\Gamma_p}{dT}}b\Delta T. \qquad (23)$$

In c-Si, $d\omega_p/dT = -0.035$ cm^{-1}/K and $d\Gamma_p/dT = +0.018$ cm^{-1}/K at 1200 K [25]. Therefore, if temperature variations in the probed volume are (incorrectly) ignored, use of the observed shift and linewidth will yield temperatures which are, respectively, much smaller and larger than T_{max}.

Simulations of the Raman spectra expected during laser heating of the 4 μm diameter polysilicon disks on fused silica and sapphire (5145 Å) were conducted assuming only temperature inhomogeneities, and are displayed in Fig. 7(a) and (b), respectively, as mentioned above. Calibration curves for fused silica and sapphire substrates were derived from these simulations and are shown in Fig. 9 in terms of ω_{pk} and Γ_{pk}, and in Fig. 10 in terms of effective temperatures. Since the thermal conductivity of silicon greatly exceeds that of fused silica at all temperatures under consideration, T_ω, T_Γ, and T_{max} are all nearly equal, as shown in Fig. 10. Furthermore, Fig. 10 dem-
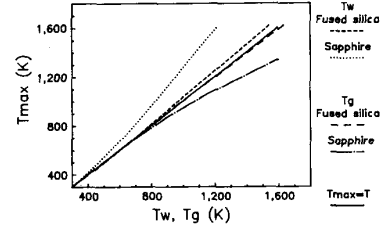

Fig. 10. The calibration curves for the maximum temperature T_{max} versus the effective temperatures T_ω (Tw in figure) and T_Γ (Tg in figure) from the simulated Raman spectra for one-beam heating of 4 μm polysilicon disks on fused silica and sapphire. Using this figure T_{max} may be derived from either effective temperature, T_ω or T_Γ.
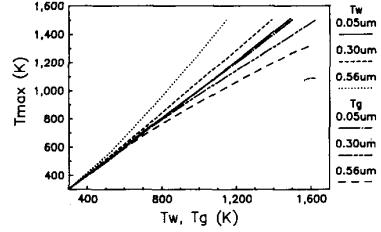

Fig. 11. T_{max} versus T_ω and T_Γ (Tw and Tg in figure) from the probe beam Raman spectrum in simulated two-beam experiments with 4 μm polysilicon disks on sapphire. Both beams impinge the disk at $r = 0$. The heating laser (5145 Å) has variable (implicit) power and a fixed spot size of 0.56 μm, while the probe beam (4880 Å) has negligible power and spot sizes of 0.05, 0.30, and 0.56 μm. (Note that in this simulation the probe beam spot size is sometimes smaller than that allowable by diffraction.)

onstrates that temperature inhomogeneities are very important in analyzing laser-heated silicon on sapphire. These curves for sapphire are qualitatively different from any in Fig. 8 because of the temperature dependence of the sapphire thermal conductivity.

Fig. 11 illustrates the importance of probe laser spot size. In this figure, conditions are similar to those used to obtain the sapphire substrate plots in Fig. 10, with the pump laser power varied implicitly and the probe laser beam radius fixed at $w_h = 0.56$ μm. However, in this case, a centrosymmetric probe laser at 4880 Å is also incident, with too little power (1 mW) to affect the temperature profile. The radius of this probe laser w_l is decreased from the one-beam value 0.56 μm, down to 0.30 and 0.05 μm, and the apparent temperatures derived from the Raman simulation frequency shift (T_ω) and linewidth (T_Γ) are plotted versus the calculated T_{max}. As expected, the effects of temperature inhomogeneities are lessened with decreasing probe beam radius. (At higher T, averaging in the z direction is always unimportant for silicon.) Because of diffraction, these simulated improvements in probing resolution are not realizable in practice, and temperature information in laser microheating with $w_h < 1$ μm must be deduced from the microprobing experiments, as described here.

B. Strain Effects

Strains in the laser-heated silicon films change the local TO phonon frequency and therefore the Raman shift. Nonuniformity in the strain within the probed volume fur-

ther broadens the Raman line. There are two sources of strain in laser heating of thin films: 1) built-in strain at ambient temperatures exists even without laser heating when the films have been deposited on substrates at elevated temperatures and when the thin film and substrate have different coefficients of thermal expansion, 2) in laser heating, there are temperature nonuniformities that produce nonuniformities in strain. This is true for the laser heating of bulk materials as well as for the heating of absorbing thin films on substrates [28].

The thermal expansion coefficient of Si ($\overline{\alpha}_{Si} = 4.0 \times 10^{-6}/°C$) is larger than that of fused silica ($\overline{\alpha}_{fused\,silica} = 0.55 \times 10^{-6}/°C$), but smaller than that of sapphire ($\overline{\alpha}_{sapphire} = 8.6 \times 10^{-6}/°C$). (Thermally averaged coefficients of thermal expansion are used here [28].) Consequently, Si films deposited on fused silica are under tensile stress at ambient temperature, while films deposited on sapphire are under compressive stress. Previous studies have shown that this causes the Raman shift for silicon thin films on fused silica [26] and on sapphire [26], [27] to be, respectively, smaller and larger than for silicon substrates, and this has been confirmed by the data reported in Section II.

Two different models are used to estimate the importance of strain effects on the Raman profile during laser heating. In the first model, the measured perturbation in the Raman profile due to built-in film strain is used to arrive at the overall perturbation in the Raman profile expected from the combined effects of built-in strain and laser heating. In the second model, built-in strain and the laser heating effects are treated independently. In both models, the local frequency shift including the effect of strain is decomposed into the shift for the unstressed material from (13) plus a perturbation due to local strain.

$$\omega_p(T) = \omega_p^{c\text{-}Si}(T) + \delta\omega_p^{strain}(T). \qquad (24)$$

The strain-induced perturbation at room temperature (T_r), $\delta\omega_p^{strain}(T_r)$ is obtained from experiments using very low probe powers described in Section II. These thin-film models are assumed to be valid for disks, and are applied directly to the cases at hand.

There is no strain when the film is deposited, so $\delta\omega_p^{strain}(T_d) = 0$ where T_d is the substrate temperature during deposition ($T_d = 640°C$ for polysilicon CVD). In model 1, it is assumed that the Raman shift due to strain is proportional to the strain magnitude; the tensor nature of strain is not considered. If the coefficient of thermal expansion of the substrate is $\overline{\alpha}_{sub}$, while that of the silicon deposit is $\overline{\alpha}_{Si}$, then

$$\delta\omega_p^{strain}(T_r) = k(\overline{\alpha}_{sub} - \overline{\alpha}_{Si})(T_r - T_d) \qquad (25)$$

where k can be determined since the other quantities are known or measured. This expression assumes that substrate thermal expansion is unaffected by the film, and that the film always adheres to the substrate. The perturbation in the Raman shift of the film due to strain when both the film and substrate are at temperature T, as in oven heating, is

$$\delta\omega_p^{strain}(T) = \frac{T - T_d}{T_r - T_d}\delta\omega_p^{strain}(T_r) \qquad (26)$$

using k derived from (25).

In model 1, the laser heats the disk to a temperature T_l locally and the substrate region near the disk to T_s, giving the perturbation in phonon frequency

$$\delta\omega_p^{strain}(T_l) = \frac{(T_s - T_d)\overline{\alpha}_{sub} - (T_l - T_d)\overline{\alpha}_{Si}}{(T_r - T_d)(\overline{\alpha}_{sub} - \overline{\alpha}_{Si})}\delta\omega_p^{strain}(T_r). \qquad (27)$$

Depending on the heating conditions, T_s may range from T_r to T_l.

In [28], the perturbation in the Raman shift in a film heated by a focused Gaussian beam laser was calculated assuming no built-in strain at room temperature. If at the center of the laser spot the temperature rises to T_l, then the perturbation in the shift of the singlet component of the Raman spectrum (which can dominate in backscattering configuration by proper choice of polarizations) at $r = 0$ is

$$\delta\omega_p^{strain,\,laser}(T_l) = \frac{1}{\omega_p^{c\text{-}Si}(T)}\left(q + \frac{\nu_{Si}}{\nu_{Si} - 1}p\right)$$
$$\cdot \left(\frac{\nu_{sub} + 1}{2}\overline{\alpha}_{sub} - \overline{\alpha}_{Si}\right)(T_l - T_r) \qquad (28)$$

where $p = -1.43 \times 10^{28}/s^2$, $q = -1.89 \times 10^{28}/s^2$, and $r = -0.59 \times 10^{28}/s^2$ [30] and ν is Poisson's ratio, 0.42 for silicon. In model 2, the total shift due to strain is given by

$$\delta\omega_p^{strain}(T_l) = \delta\omega_p^{strain}(T_r) + \delta\omega_p^{strain,\,laser}(T_l). \qquad (29)$$

These models are compared in Table I for the case with the laser heating the silicon disk to the melting point, 1690 K, for both fused silica and sapphire substrates; the strain-induced corrections should be largest at this high temperature. The two extremes of model 1 are considered by choosing the substrate temperature alternately equal to the disk or the ambient temperature. For silicon on fused silica, the two variations of model 1 give consistent values, which are also roughly equal to the predictions of model 2. Model 1 does make somewhat different predictions for the different size disks. Apparently, the exclusion of strain effects in the Raman shift can lead to an underestimate of the temperature by about 60–100 K for silicon on fused silica.

The importance of strains in Raman analysis of silicon films on sapphire is less clear. Model 2 suggests that the temperature determination is unaffected by laser-heating-induced strain. The two versions of model 1 give temperature shifts on the order of 50 K, but with opposite signs. Because the temperature profile during focused laser heating of silicon on sapphire is inhomogeneous, the substrate

TABLE I
STRAIN-INDUCED PERTURBATIONS IN RAMAN SHIFT AND RAMAN-DERIVED TEMPERATURE

	$\delta\omega_p(T_r)$ (cm⁻¹)	$\delta\omega_p(T_l = 1690\text{ K}) - \delta\omega_p(T_r)$ (cm⁻¹)		
		Model 1 with $T_s = T_r = 295$ K	Model 1 with $T_s = T_l = 1690$ K	Model 2
Diameter of poly-1 silicon disk on fused quartz				
4 μm	−1.0	2.6 (63)	2.3 (54)	2.6 (62)
13 μm	−1.6	4.2 (100)	3.6 (86)	2.6 (62)
23 μm	−1.9	5.0 (119)	4.3 (102)	2.6 (62)
Diameter of poly-1 silicon disk on sapphire				
4 μm	0.6	1.2 (28)	−1.4 (−32)	−0.15 (−4)
13 μm	1.3	2.5 (60)	−2.9 (−70)	−0.15 (−4)
23 μm	1.6	3.1 (74)	−3.6 (−86)	−0.15 (−4)

A positive value means that inclusion of strain increases the value of the temperature derived from the Raman profile.
The second column gives the difference between the measured Raman frequency for the disk and that of c-Si. The third to fifth columns give the frequency shifts due to laser heating induced strains in cm⁻¹. In parentheses is the change in determined temperature (K) when these strains are included in the analysis.

temperature near the disk will be between the ambient and disk temperature. Therefore, the correct prediction for the Raman shift correction due to strain may well be between the two model 1 predictions, and therefore very small like the model 2 prediction.

Strains also influence the linewidth of the Raman line. In analogy with the discussion of Raman shifts, there is a contribution to the width at ambient temperature from film deposition:

$$\Gamma_p(T) = \Gamma_p^{\text{c-Si}}(T) + \delta\Gamma_p^{\text{strain}}(T_r) \qquad (30)$$

where $\delta\Gamma_p^{\text{strain}}(T_r)$ is the measured added linewidth at room temperature, as given in Section II. Furthermore, strains within the volume probed by the laser are not uniform because of the nonuniformities in the temperature profile, and this leads to additional line broadening. This is automatically included in this formulation by using the strain-perturbed Raman frequency, from either (27) or (29), in (17).

C. Photocreated Carrier Effects

Free carriers in silicon can perturb the Raman spectrum near the optical phonon peak in silicon because of Fano-like interference between optical phonon scattering and continuum interband electronic scattering [30], [31]. In c-Si, this free carrier scattering effect is particularly strong for holes, especially at concentrations above $10^{20}/\text{cm}^3$, and can lead to excessively broadened and highly asymmetric profiles near the 520 cm⁻¹ peak at ambient temperature [31].

In both laser heating and laser probing of silicon, the electron–hole pair density ρ can greatly exceed the concentration expected in intrinsic material at the local temperature. The thermal pair density ρ_T is $1.3 \times 10^9/\text{cm}^3$ at 300 K, $2.2 \times 10^{17}/\text{cm}^3$ at 1000 K, and $8.2 \times 10^{18}/\text{cm}^3$ at 1600 K [32]. At high laser intensities, the electron–hole pair density is obtained by equating the rate of production of pairs by absorption to the rate of recombination. For

large ρ, Auger recombination is the fastest loss term.

$$\rho_L = \left(\frac{\alpha I}{\hbar\omega C}\right)^{1/3} \qquad (31)$$

where α is the absorption coefficient, I is the laser intensity, and C is the Auger recombination rate, $\sim 2 \times 10^{-31}$ cm⁶/s for silicon [33]. Equation (31) is valid only when $\rho_L \gg \rho_T$.

For typical probing conditions for silicon on sapphire, $P = 1$ mW and $w = 0.56$ μm, the concomitant temperature rise is small, < 10 K, and $\rho_L = 2.7 \times 10^{19}/\text{cm}^3$ is much larger than the thermal electron–hole pair density $\rho_T < 3 \times 10^9/\text{cm}^3$. With increasing laser power, ρ_L increases as $P^{1/3}$ and still always exceeds ρ_T, which nonetheless increases relatively much faster. When $P \sim 75$ mW, the silicon temperature reaches 1000 K, and $\rho_T = 2.2 \times 10^{17}/\text{cm}^3$, while $\rho_L = 1.9 \times 10^{20}/\text{cm}^3$, and when $P \sim 100$ mW, $T = 1600$ K, with $\rho_T = 8.2 \times 10^{18}/\text{cm}^3$ and $\rho_L = 3.4 \times 10^{20}/\text{cm}^3$.

If under a given set of experimental conditions, the density of electron–hole pairs is near the thermal equilibrium value, any line broadening at the Si optical phonon peak due to free carriers is automatically included in (14). If photon creation of electron–hole pairs dominates, then to first order, electronic Raman scattering due to electron–hole pairs can be treated by considering the independent perturbations of the holes and electrons. When the hole concentration due to doping in c-Si is $1.6 \times 10^{20}/\text{cm}^3$, these effects can increase the linewidth by ~ 12 cm⁻¹ for Raman excitation at 4880 Å [31]. Such effects have also been considered in the Raman analysis of laser-heated silicon by Compaan *et al.* [7].

The importance of photocreated carriers was examined here experimentally using cofocused beams from an argon-ion laser at 5145 Å (0–100 mW), to create electron–hole pairs in a 4 μm diameter epi-Si disk on sapphire, and a krypton-ion laser at 6471 Å (~ 100 mW, which is weakly absorbed [19]), to probe this distribution. Under these conditions, the green laser creates carriers with min-

imal temperature rise. Because of the large phonon/electronic continuum Raman interference for longer wavelengths [31], this krypton–ion laser line is a sensitive probe of free carrier-induced perturbations. However, no evidence of increased linewidth or asymmetry was observed in these experiments, except for the increase in linewidth that occurred when the power of the 5145 Å beam was raised enough to heat the disk appreciably.

This null observation can be explained by the different conditions encountered in [30] and [31], and those encountered here. Those studies were conducted in unstressed c-Si, and the observed interference was caused by the large contribution in the electronic continuum scattering near 520 cm^{-1}. This electronic Raman continuum was large at 520 cm^{-1} because of the combined effects of the small energy gap between the split-off valence bands at the Γ point and the nonparabolicity of the valence bands. Nonhydrostatic strain due to the built-in stress of the silicon disks on the substrates and, at higher laser powers, also due to the stresses from localized laser heating can increase the gap between the valence bands and also make them more parabolic. Both of these effects can decrease the electronic Raman contribution at the optical phonon peak frequency, as was demonstrated in [31] with the application of uniaxial stress. Consequently, photon-created electron–hole pairs probably have negligible influence on the Raman spectra in this study.

V. Comparison of Experiments and Simulations

The point of comparison between the one-beam experiment and the model is the maximum temperature T_{max} in the temperature distribution. For a given experiment, the expected temperature profile can be calculated using known parameters, as demonstrated in Section III, to obtain the computed value of T_{max}. The measured value of T_{max} is obtained by applying the appropriate calibration curve to the measured spectrum, using T_ω (or equivalently, ω_{pk}) or instead T_Γ (or equivalently, Γ_{pk}) to obtain T_{max}; the same value of T_{max} should be derived using either the frequency shift or the linewidth calibration. Fig. 10 has the appropriate correction plots for the 4 μm polysilicon disk experiments on fused silica and sapphire if no other perturbations, such as those due to strain, are included. Once T_{max} has been obtained from one-beam experiments, the temperature profile can be derived using the calculated temperature profiles.

Fig. 12 shows T_{max} in the laser heating experiments for the 4 μm polysilicon disks on fused silica presented in Fig. 2. T_{max} is obtained from the heat flow calculations (straight line), and from the observed spectra using the simulation spectrum frequency shift correction (circles, from T_ω or ω_{pk}) or linewidth correction (squares, from T_Γ or Γ_{pk}). These corrections include built-in stress contributions to the lineshape, but not the temperature-dependent strain effects described in Section IV-B. The observed melting condition is also plotted. There is fairly good agreement between the measured and calculated maximum profile temperature, the former being higher by about 100 K near melting (1690 K). The experimental T versus laser power plot extrapolates to the observed

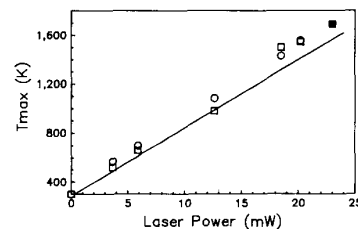

Fig. 12. Comparison of T_{max} obtained from the temperature calculation (solid lines) and the experimental Raman profiles (from Fig. 2), using T_ω (open circles) or T_Γ (open squares) from the Raman simulations (Fig. 10), versus laser power for 4 μm polysilicon disks on fused silica. The experimental melting point is also plotted (filled square).

melting condition. Using Table I, the temperature-dependent strain effects would seemingly increase the "observed" temperature determined from the frequency shift by about 60 K for T_{max} near melting.

Fig. 13 shows a similar comparison (using only built-in strain corrections) for the 4 μm diameter poly-2 disks on sapphire. Again, the agreement between experiment and calculation is good, as is agreement of the extrapolated experimental curve with the melting condition. Despite the large temperature inhomogeneities within the probed volume, both the Raman shift and linewidth data give essentially the same T_{max} after following the procedures in Section IV.

Using the frequency shifts and linewidths for one-beam heating and probing of 4 μm poly-1, poly-2, and epi silicon disks on sapphire, T_{max} is obtained and shown in Fig. 14; the frequency shifts and linewidths give consistent values of T_{max} in each example. In each case, the measured temperatures again extrapolate to the melting condition; this is not explicitly shown in the figure for the epi silicon case. However, agreement with the calculated T_{max} is not universal. As demonstrated in Fig. 13, the poly-2 experiments and calculation agree. Although the calculated temperatures for the poly-1 experiment are essentially the same as for the poly-2 example, the observed temperature rises for poly-1 are consistently about 20 percent higher than these predictions. Known differences in the geometry and in the thermal and optical properties of the deposit and substrate in the two polysilicon on sapphire cases are insufficient to explain this deviation. Perhaps the excessive strain in the poly-1 samples relative to poly-2, exhibited by its much broader Raman lineshape at low laser power, is the reason for this difference. The calculations of laser heating of epi silicon disks on sapphire give temperatures that are consistently higher than those from the Raman measurements, and these values are only slightly lower than those predicted for poly-2 structures at equivalent laser powers. It is possible that increased thermal conductivity due to photocreated electron–hole pairs, which could be important in these (epi) silicon disks without grain boundaries, may account for this. Because the Raman-derived temperatures are consistent with the melting data, the Raman determination of temperature is probably superior to the temperature calculation in these exceptional cases.
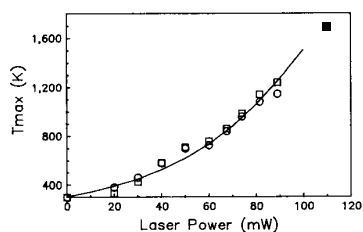
For a given laser power and spot size, the laser-induced

Fig. 13. Comparison of T_{max} obtained from the temperature calculation (solid lines) and the experimental Raman profiles (from Fig. 3), using T_ω (open circles) or T_Γ (open squares) from the Raman simulations (Fig. 10), versus laser power for 4 μm polysilicon disks on sapphire. The experimental melting point is also plotted (filled square).
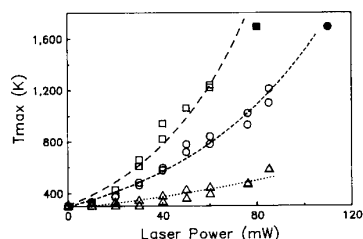

Fig. 14. Comparison of T_{max} obtained from Raman analysis during the laser heating of 4 μm diameter poly-1 (open squares), poly-2 (open circles), and epi (open triangles) disks on sapphire, using both the frequency shift and linewidth determinations from the Raman simulations. The observed melting condition for the two poly cases are noted by the filled-in symbols; for the epi sample, melting occurred with 300 mW.

disk radius when $K_d \gg K_s$, and is expected to be relatively independent of disk radius when the deposit and substrate have comparable thermal conductivity [22]. This explains the trends observed in Figs. 2 and 3. With the fused silica substrate, increasing the disk radius leads to a large decrease in temperature rise as demonstrated by the variation of Raman shifts and linewidths with laser power, as plotted in Fig. 2. For the sapphire substrate, the increase in disk size is seen to have a very small effect on the temperature rise induced by the laser in Fig. 3; this appears to be even a smaller effect than suggested by temperature calculations.

The two-beam heating and probing experiments on 13 μm poly-1 disks presented in Fig. 4 can now be interpreted in terms of temperature profiles. For the fused silica substrate, both frequency shift and linewidth determination of temperature give a temperature of about 1150 K at the center, which decreases to about 600 K at a displacement of 3 μm from the center and remains at this temperature to the end of the disk. For the sapphire case, the temperature is about 1100 K at the center, again both from phonon frequency and linewidth measurements, and decreases rapidly with displacement from the center to near ambient temperature, 350–450 K, with most of the temperature drop occurring within a micrometer of center. As also suggested by the calculations portrayed in Fig. 6, the relatively low thermal conductivity of the fused silica substrate compared to that of sapphire is exemplified by the relatively slow decrease of temperature with displacement from the center and the relatively high temperature at the disk periphery, as well as by the relatively low laser powers needed to achieve comparable T_{max} for the fused silica substrate vis-à-vis sapphire.

The accuracy of the Raman simulations depends on the completeness and accuracy of the available optical constants. In this study, the published values of the Raman frequencies and linewidths, reflectivity, and absorption coefficients in silicon have been extrapolated to higher temperatures, as needed. Furthermore, one particular expression for the Raman susceptibility was used here [23]; alternative forms are also available [24]. The normalized simulated Raman lineshapes, and therefore also the deduced temperatures, are not very sensitive to the exact form of the susceptibility.

VI. CONCLUSIONS

When properly analyzed, one-beam Raman microprobe spectra can be used to determine the maximum temperature and the temperature distribution in the probed region, even when microstructures are heated with submicron dimension beams. Correction for temperature inhomogeneity within the probed volume is very important, and can be attained for arbitrary microstructure geometry and materials by deriving and then using the appropriate calibration curve. Although in some cases stress effects are of secondary importance, if ignored they can sometimes lead to 5–10 percent errors in the determined laser-induced temperature rise. Perturbations due to photon-created electrons and holes can be ignored in silicon when there is large nonhydrostatic stress, as is true here.

The precision of the Raman temperature measurements is sufficient for many real-time monitoring applications in which reproducibility of processing conditions is necessary. The accuracy of the temperature rise appears to be ≤ 100 K near the melting temperature of silicon, based on agreement with the laser melting condition for both fused silica and sapphire substrates. The temperature calculations are in agreement with measurements for silicon disks on fused silica substrates, but there are differences between measurements and calculations for laser-heated disks on sapphire substrates, probably because of the use of incorrect thermal or optical parameters in the calculations.

Use of a second focused laser, focused as tightly as allowed by diffraction, as a scannable probe of laser microheating leads to a better determination of the temperature profile than finding T_{max} and coupling it to calculated temperature profiles in one-beam heating and probing.

ACKNOWLEDGMENT

The authors would like to thank G. E. Jellison for useful conversations.

REFERENCES

[1] I. P. Herman, "Direct-laser writing," in *Photochemical Materials Processing*, K. G. Ibbs and R. M. Osgood, Ed. Cambridge: Cambridge Univ. Press, 1989, pp. 61–108.

[2] D. Bauerle, *Chemical Processing with Lasers*. Berlin: Springer, 1986.

[3] Y. Rytz-Froidevaux, R. P. Salathe, and H. H. Gilgen, "Laser generated microstructures," *Appl. Phys.*, vol. A37, pp. 121–138, 1985.

[4] H. W. Lo and A. Compaan, "Raman measurements of temperature during cw laser heating of silicon," *J. Appl. Phys.*, vol. 51, pp. 1565–1568, 1980.

[5] D. Kirillov and J. L. Merz, "Raman scattering as a temperature probe

for laser heating of Si," *Mater. Res. Soc. Symp. Proc.*, vol. 17, pp. 95-102, 1983.

[6] J. Raptis, E. Liarokapis, and E. Anastassakis, "Effects of temperature gradients on the first-order Raman spectrum of Si," *Appl. Phys. Lett.*, vol. 44, pp. 125-127, 1984.

[7] A. Compaan, M. C. Lee, and G. J. Trott, "Phonon populations by nanosecond-pulsed Raman scattering in Si," *Phys. Rev.*, vol. B32, pp. 6731-6741, 1985.

[8] M. Yamada, K. Nambu, Y. Itoh, and K. Yamamoto, "Raman microprobe study on temperature distribution during cw laser heating of silicon on sapphire," *J. Appl. Phys.*, vol. 59, pp. 1350-1354, 1986.

[9] F. Magnotta and I. P. Herman, "Raman microprobe analysis during the direct laser writing of silicon microstructures," *Appl. Phys. Lett.*, vol. 48, pp. 195-197, 1986.

[10] I. P. Herman, F. Magnotta, and D. E. Kotecki, "Direct-laser writing of silicon microstructures: Raman microprobe diagnostics and modeling of the nucleation phase of deposition," *J. Vac. Sci. Technol.*, vol. A4, pp. 659-664, 1986.

[11] G. D. Pazionis, H. Tang, L. Ge, and I. P. Herman, "Stokes/anti-Stokes Raman microprobe analysis of laser-heated silicon microstructures on silicon dioxide," *Mater. Res. Soc. Symp. Proc.*, vol. 101, pp. 113-118, 1988.

[12] D. E. Kotecki and I. P. Herman, "A real time Monte Carlo simulation of thin film nucleation in localized-laser chemical vapor deposition," *J. Appl. Phys.*, vol. 64, pp. 4920-4942, 1988.

[13] R. C. Weast, Ed., *CRC Handbook of Chemistry and Physics*. Boca Raton, FL: CRC, 62nd ed., 1981.

[14] Y. S. Touloukian, Ed., *Thermophysical Properties of High Temperature Solid Materials*. New York: Macmillan, 1967, vol. 4, p. 359.

[15] Y. S. Touloukian, Ed., *Thermophysical Properties of High Temperature Solid Materials*. New York: Macmillan, 1967, vol. 4, p. 45.

[16] Y. S. Touloukian and R. W. Powell, Ed., *Thermophysical Properties of Matter*. New York: lFl Plenum, 1980, vol. 1.

[17] T. Kamins, *Polycrystalline Silicon for Integrated Circuit Applications*. Boston: Kluwer, 1988.

[18] J. E. Moody and R. H. Hendel, "Temperature profiles induced by a scanning cw laser beam," *J. Appl. Phys.*, vol. 53, pp. 4364-4371, 1982.

[19] G. E. Jellison, Jr. and F. A. Modine, "Optical absorption of silicon between 1.6 and 4.7 eV at elevated temperatures," *Appl. Phys. Lett.*, vol. 41, pp. 180-182, 1982.

[20] G. Lubberts, B. C. Burkey, F. Moser, and E. A. Trabka, "Optical properties of phosphorus-doped polycrystalline silicon layers," *J. Appl. Phys.*, vol. 52, pp. 6870-6878, 1981.

[21] G. Harbeke, L. Krausbauer, E. F. Steigmeier, A. E. Widmer, H. F. Kappert, and G. Neugebauer, "Growth and physical properties of LPCVD polycrystalline silicon films," *J. Electrochem. Soc.*, vol. 131, pp. 675-682, 1984.

[22] K. Piglmayer, J. Doppelbauer, and D. Bauerle, "Temperature distributions in cw laser induced pyrolytic deposition," *Mater. Res. Soc. Symp. Proc.*, vol. 29, pp. 47-54, 1984.

[23] G. E. Jellison, D. H. Lowndes, and R. F. Wood, "Importance of temperature-dependent optical properties for Raman-temperature measurements for silicon," *Phys. Rev.*, vol. B28, pp. 3272-3276, 1983.

[24] A. Compaan and H. J. Trodahl, "Resonance Raman scattering in Si at elevated temperatures," *Phys. Rev.*, vol. B29, pp. 793-801, 1984.

[25] M. Balkanski, R. F. Wallis, and E. Haro, "Anharmonic effects in light scattering due to optical phonons in silicon," *Phys. Rev.*, vol. B28, pp. 1928-1934, 1983.

[26] F. Moser and R. Beserman, "Stress relief in heavily doped silicon layers," *J. Appl. Phys.*, vol. 54, pp. 1033-1036, 1983.

[27] T. Englert, G. Abstreiter, and J. Pontcharra, "Determination of existing stress in silicon films on sapphire substrate using Raman spectroscopy," *Solid State Electron.*, vol. 23, pp. 31-33, 1980.

[28] L. P. Welsh, J. A. Tuchman, and I. P. Herman, "The importance of thermal stresses and strains induced in laser processing with focused Gaussian beams," *J. Appl. Phys.*, vol. 64, pp. 6274-6286, 1988.

[29] J. Gonzalez-Hernandez, G. H. Azarbayejani, R. Tsu, and F. H. Pollak, "Raman, transmission electron microscopy, and conductivity measurements in molecular beam deposited microcrystalline Si and Ge: A comparative study," *Appl. Phys. Lett.*, vol. 47, pp. 1350-1352, 1985.

[30] M. Chandrasekhar, J. B. Renucci, and M. Cardona, "Effects of interband excitations on Raman phonons in heavily-doped n-Si," *Phys. Rev.*, vol. B17, pp. 1623-1633, 1978.

[31] F. Cerdeira, T. A. Fjeldly, and M. Cardona, "Effect of free carriers on zone-center vibrational modes in heavily doped p-type Si. II. Optical modes," *Phys. Rev.*, vol. B8, pp. 4734-4745, 1973; and M. Chandrasekhar, private communication.

[32] S. M. Sze, *Physics of Semiconductor Devices*. New York: Wiley, 2nd ed., 1981.

[33] J. Dziewior and W. Schmid, "Auger coefficients for highly doped and highly excited silicon," *Appl. Phys. Lett.*, vol. 31, pp. 346-348, 1977.
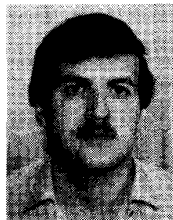
Gregory D. Pazionis was born on June 10, 1958, in Athens, Greece. He received the physical sciences degree from the University of Athens, Athens, Greece, in 1981, the M.S. degree in physics from Boston College, Boston, MA, in 1983, and the Dr.rer.nat. degree from the Technical University of Berlin, Berlin, West Germany, in 1986. His doctoral thesis was on studies of radiation damage processes in II-VI compounds using laser spectroscopy and cathodoluminescence.

From January 1987 to April 1988 he was an IBM Postdoctoral Research Scientist with the Department of Applied Physics, Columbia University, New York, where he conducted research on the characterization of silicon on insulator microstructures with Raman microprobe techniques and on laser-assisted surface processing. Since July 1988, he has been a Senior Engineer with the Device Development group at Lasertron, Burlington, MA. He is currently investigating degradation mechanisms of semiconductor lasers using cathodoluminescence, electroluminescence, EDX, and EBIC.

Dr. Pazionis is a member of the American Physical Society and the Materials Research Society.

Hua Tang was born in Beijing, China, on January 12, 1957. He received the B.S. degree in physics from Tsinghua University, Beijing, China, in 1982 and the M.S. degree in quantum electronics from Columbia University, New York, in 1988.

From 1982 to 1986 he was a teaching assistant with the Department of Physics, Tsinghua University. He is currently working towards the Ph.D. degree in quantum electronics at Columbia University. His research interests include laser diagnostics and laser-controlled chemical processing on surfaces of semiconductors and metals.

Mr. Tang is a member of the Material Research Society.
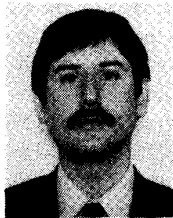
Irving P. Herman (M'87) was born on October 18, 1951, in Brooklyn, NY. He received the B.S. and Ph.D. degrees in physics from the Massachusetts Institute of Technology, Cambridge, in 1972 and 1977, respectively. While doing his doctoral research involving laser chemistry and spectroscopy, he was a Fannie and John Hertz Foundation Fellow. During his stay at M.I.T., he was also involved with the early efforts on optically-pumped infrared lasers and Dicke superradiance.

In 1977 he joined the Lawrence Livermore National Laboratory where he later became a section leader, and worked on laser isotope separation of deuterium and tritium, laser microchemical processing of surfaces and its applications in microelectronics, and Raman microprobe analysis. In 1986 he joined Columbia University, New York, as an Associate Professor of Applied Physics. His current research interests include optical diagnostics of thin film processing, laser processing of microelectronics materials, laser spectroscopy of semiconductor microstructures, modeling the interaction of lasers with materials, and the physics of semiconductors under high pressure. He is also affiliated with the Columbia Radiation Laboratory and the Microelectronics Sciences Laboratories.

Dr. Herman is a member of the American Physical Society and the Materials Research Society. He has organized several meetings on the applications of lasers, including the 1987 Materials Research Society symposium of laser chemical processing of surfaces.